SUPPLEMENTAL MATERIALS

Lymphatic and immune cell cross-talk regulates cardiac recovery after experimental myocardial infarction

Houssari M[1], Dumesnil A[1], Tardif V[1], Kivela R[4], Pizzinat N[5], Boukhalfa I[1], Godefroy D[2], Schapman D[3], Hemanthakumar KA[4], Bizou M[5], Henry JP[1], Renet S[1], Riou G[6], Rondeaux J[1], Anouar Y[2], Adriouch S[6], Fraineau S[1], Alitalo K[4], Richard V[1], Mulder P[1], Brakenhielm E[1]

[1]Normandy University, UniRouen, Inserm (Institut National de la Santé et de la Recherche Médicale) UMR1096 (EnVI Laboratory), FHU REMOD-VHF, Rouen, France

[2]Normandy University, UniRouen, Inserm UMR1239 (DC2N Laboratory), Mont Saint Aignan, France

[3]Normandy University, UniRouen, PRIMACEN, Mont Saint Aignan, France

[4]Wihuri Research Institute and Translational Cancer Biology Program, Research Programs Unit, Faculty of Medicine, University of Helsinki, Helsinki, Finland

[5]Institut des Maladies Métaboliques et Cardiovasculaires (I2MC), Inserm UMR1048, Université de Toulouse III, Toulouse, France

[6]Normandy University, UniRouen, Inserm (Institut National de la Santé et de la Recherche Médicale) UMR1234 (PANTHER Laboratory), Rouen, France

Supplemental figures

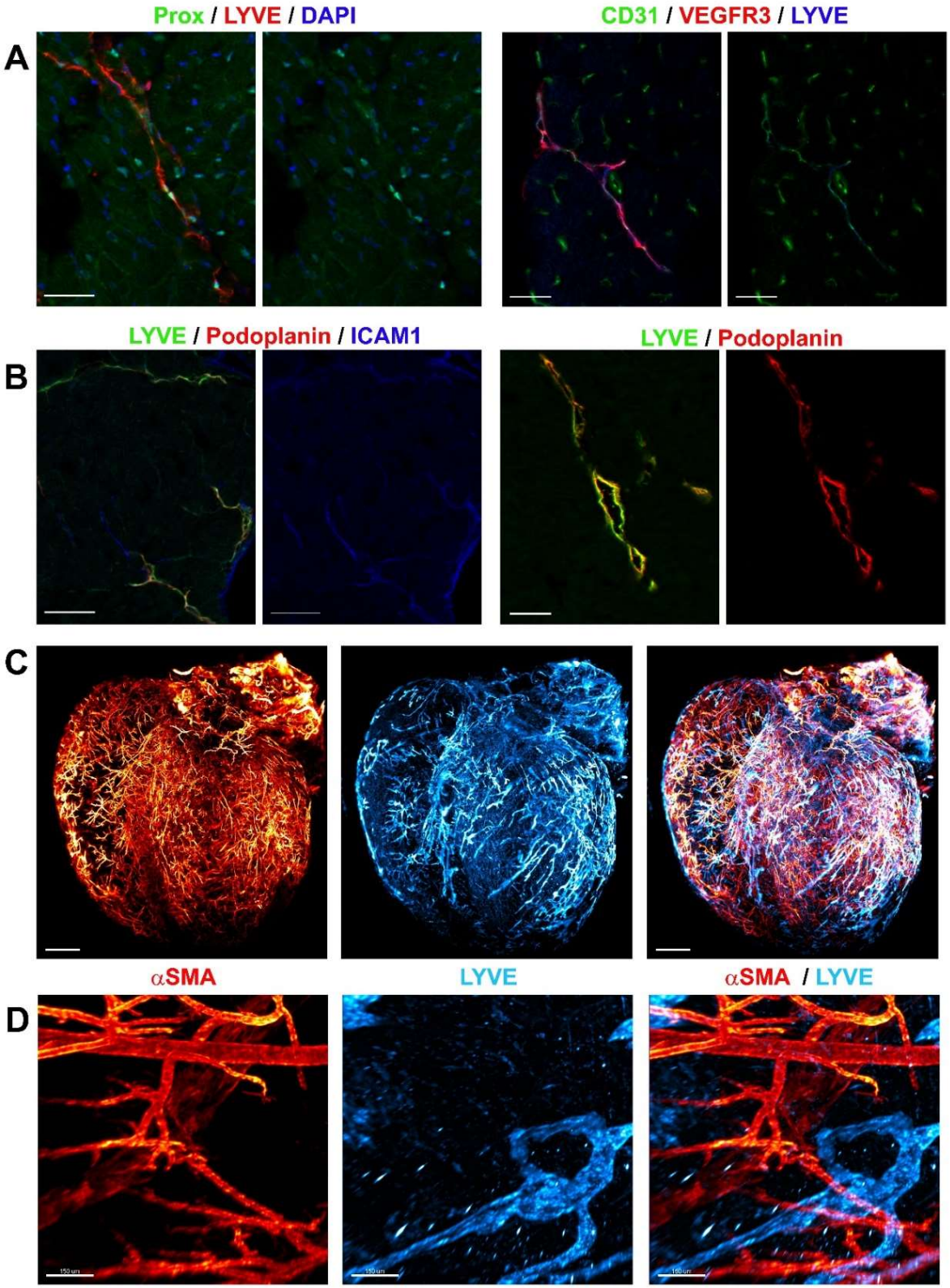

Suppl. Fig. I Cardiac lymphatic markers in healthy mouse hearts

Immunohistochemical analyses of cardiac sections demonstrate that LYVE-1^{+} healthy adult female mouse subepicardial lymphatic vessels express prox-1, VEGFR3, and podoplanin (**a**, **b**). They further weakly express ICAM1. *x20* magnification, scale bar = 50 µm. Evaluation by lightsheet (**c**, *x0.8,* scale bar 1 mm) and confocal (**d**, *x20,* scale bar 50 µm) microscopy of a whole mount-stained healthy adult female mouse heart reveals a dense lymphatic network (Lyve1, *blue*) on the epicardial surface, where lymphatics run next to blood vessels (smooth muscle alpha actin, *red*). Note absence of smooth muscle cell-coating on cardiac lymphatics (**d**).

Suppl. Video Lymphatic network is restricted to outer cardiac layers in mice

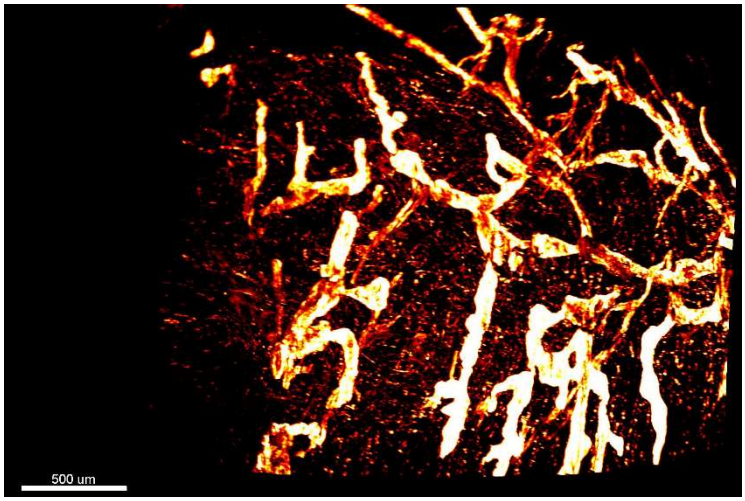

Lightsheet imaging of cardiac whole mount stained for Lyve1: Cardiac lymphatics are essentially restricted to the outer surface of the heart in healthy mice. Scalebar 500 µm.

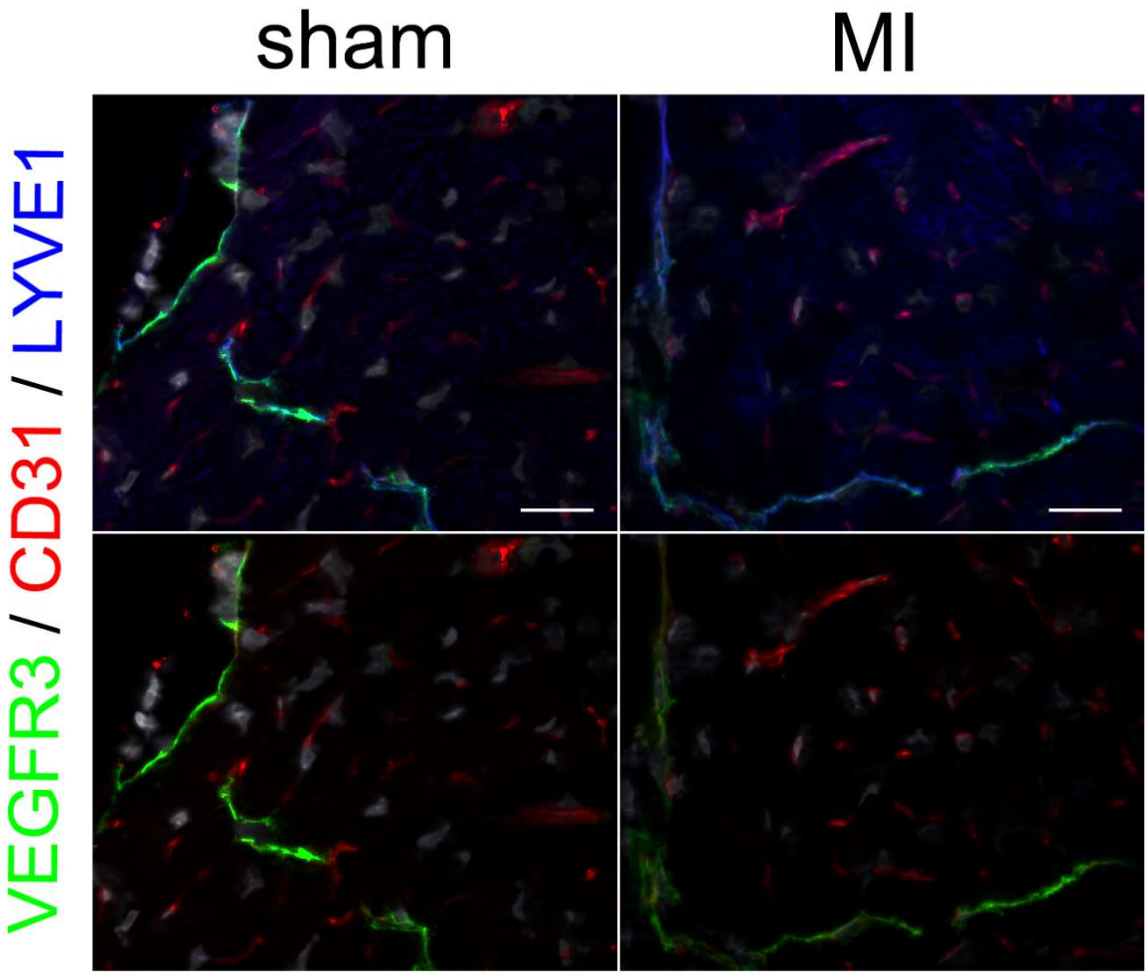

Suppl. Fig. II Lymphatic-selective expression of VEGFR3 is maintained in the heart post-MI

Immunohistochemical analyses of cardiac sections demonstrate that VEGFR3 expression (*green*) is restricted to lymphatics (LYVE1, *blue*), and not blood vessels (CD31, *red*), in healthy sham-operated mice and in mice at 7 days post-MI. Scale bar = 50 μm.

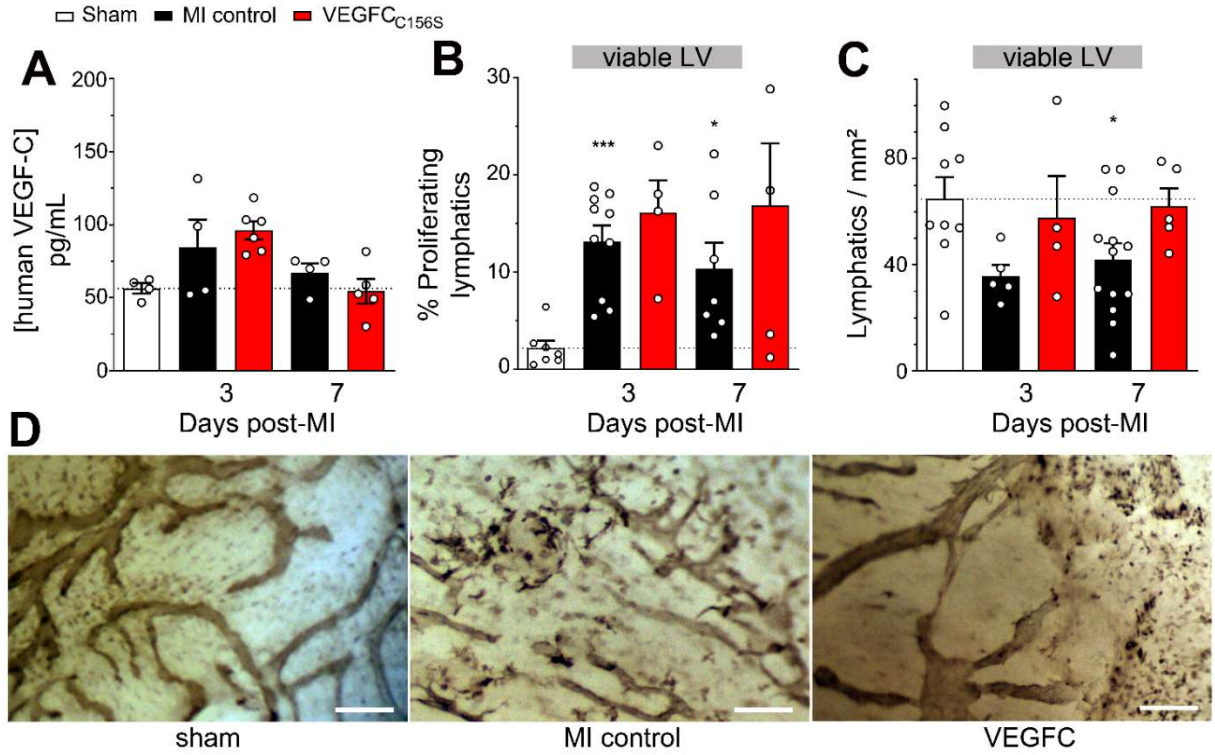

Suppl. Fig. III Intraperitoneal VEGF-C$_{C156S}$ protein therapy does not increase cardiac lymphangiogenesis in mice post-MI

Mice were treated by repeated intraperitoneal injection of 2 microgram rhVEGF-C$_{C156S}$ (*red*, *n=5*) on days 0, 2, 3, 4, and 6 post-MI. MI controls were injected with physiological saline (*black*, *n=7-13),* and sham-operated mice (*white*, *n=7-9*) served as healthy controls. Circulating recombinant human VEGF-C plasma levels were determined by ELISA (**a**), and cardiac lymphangiogenesis was evaluated as % proliferating lymphatic vessels (**b**) and lymphatic densities (**c**) in non-infarcted viable LV at 3 and 7 days post-MI. Examples of day 3 peri-infarct lymphatics (LYVE1, *brown*). Scale bar = 50 µm. Kruskal-Wallis followed by Dunn's posthoc test. *, p<0.05; ***, p<0.001 *vs*. sham.

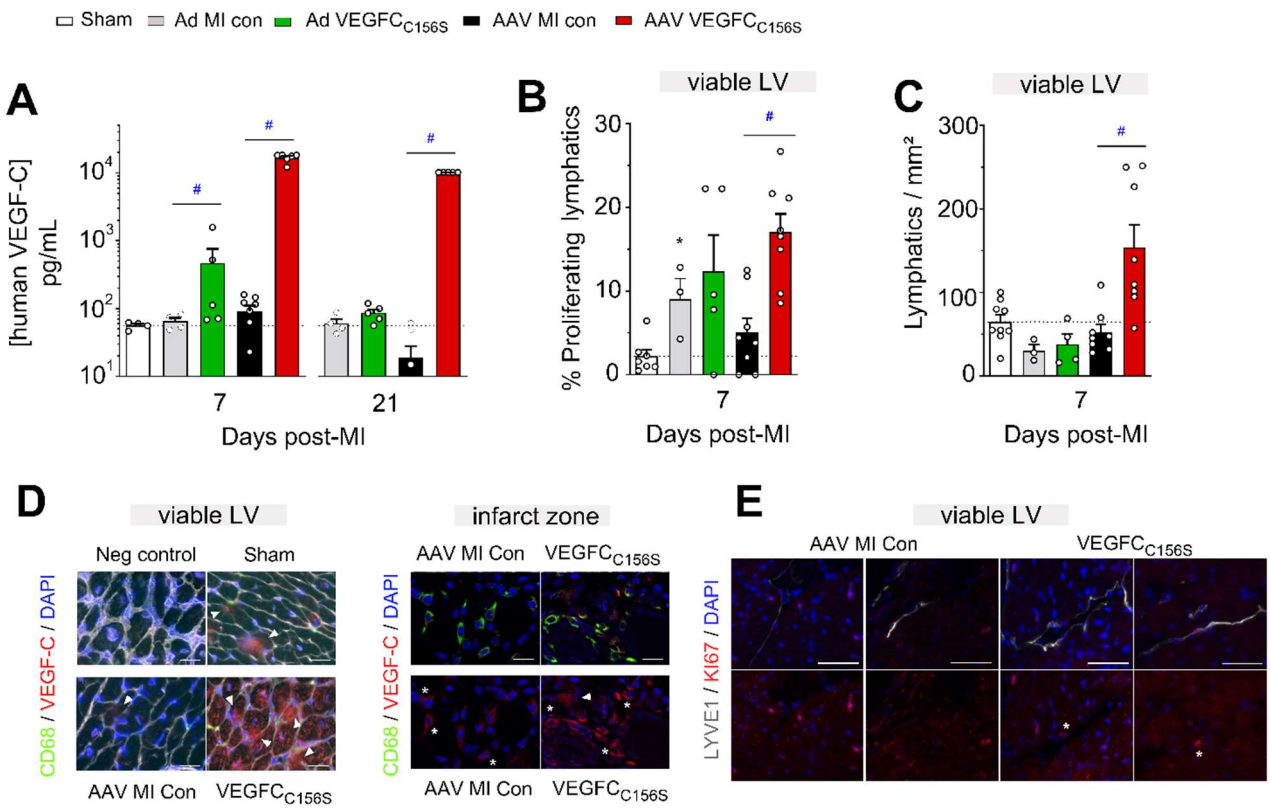

Suppl. Fig. IV AAV gene delivery, but not Adenoviral gene delivery, of VEGF-C$_{C156S}$ durably increases circulating VEGF-C levels in mice post-MI and stimulates cardiac lymphangiogenesis

Comparison of lymphangiogenic gene therapy with either Ad-hVEGF-C$_{C156S}$ (*green*, *n=5*) or AAV-hVEGF-C$_{C156S}$ (*red*, *n=8*). MI controls were injected with either Ad-lacZ (*grey*, *n=3-5)* or AAV-scrambled virus (*black, n=8*), and sham-operated mice (*white*, *n=7-9*) served as healthy controls. Circulating VEGF-C plasma levels were determined by ELISA (**a**). Lymphangiogenesis in the viable LV wall bordering the infarct was evaluated as % proliferating lymphatic vessels (**b**) and lymphatic densities at 7 days post-MI (**c**). Examples of immunohistochemical detection of cardiac VEGF-C expression in viable LV or infarct zone at 7 days post-MI in healthy sham-operated mice, MI controls (AAV-scramble) and VEGFC (AAV-hVEGF-C$_{C156S}$)-treated mice (**d**). Negative controls included omission of anti-VEGFC antibody. VEGF-C (*red*), macrophages (*green, CD68*), nuclei (*blue*), scale bar = 20 µm. Cardiomyocytes (*white arrowhead*) produce VEGFC in healthy as well as post-MI mouse hearts. Please note VEGFC-expressing macrophages in the infarct (*white asterix*). Examples of Lyve1^{+} (*grey*) Ki67^{+} (*red*) proliferating cardiac lymphatic vessels in the viable LV in AAV MI controls and AAV VEGFC$_{C156S}$-treated mice at 7 days post-MI (**e**). *x20* magnification, scale bar = 50 µm. White asterix point to proliferating vessels.

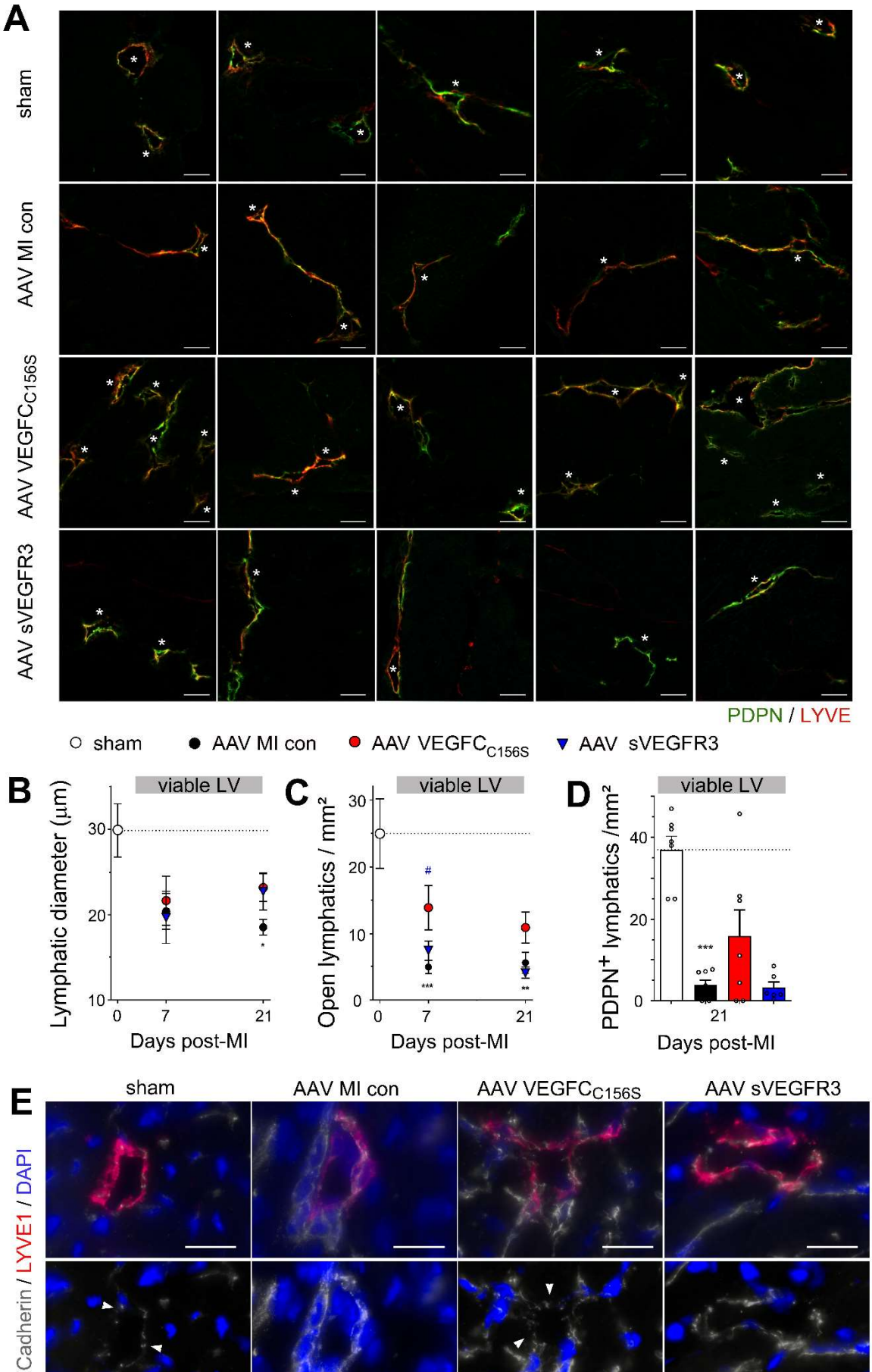
A
sham
AAV MI con
AAV VEGFC$_{C156S}$
AAV sVEGFR3
PDPN / LYVE
sham
AAV MI con
AAV VEGFC$_{C156S}$
AAV sVEGFR3
B
viable LV
Lymphatic diameter (μm)
Days post-MI
C
viable LV
Open lymphatics / mm²
Days post-MI
D
viable LV
PDPN⁺ lymphatics /mm²
Days post-MI
E
sham
AAV MI con
AAV VEGFC$_{C156S}$
AAV sVEGFR3
VECadherin / LYVE1 / DAPI

Suppl. Fig. V AAV delivery of VEGF-C_{C156S} stimulates cardiac lymphangiogenesis in the viable LV in mice post-MI

Evaluation of open lymphatic vessels in viable LV subepicardium (**a**) in healthy mice or at 21 days post-MI. Podoplanin (*green*), LYVE1 (*red*), *x20* magnification, scale bar = 50 µm. Open vessels indicated by white asterix. Quantification of lymphatic vessel diameters (**b**), open lymphatic density (**c**) and podoplanin$^+$ vessel density (**d**) in sham-operated mice (*white*, *n=7-9*), MI controls (AAV-scrambled virus, *black n=8*), VEGFC-treated mice (AAV-hVEGFC$_{C156S,}$ *red*, *n=8*), and sVEGFR3-treated mice (AAV-sVEGFR3, *blue, n=6-8*). Examples of lymphatic barrier remodeling (**e**) in viable LV at 7 days post-MI visualized by VE-cadherin (*grey*), LYVE1 (*red*), and DAPI (*blue*), *x20* magnification, scale bar = 20 µm. White arrowheads point to button-like junctions. One-way ANOVA, followed by Bonferroni for groups at 7 days post-MI, and Kruskal-Wallis followed by Dunn's posthoc test for groups at 21 days post-MI. *, p<0.05; **, p<0.01; ***, p<0.001 *vs*. sham; $, p=0.07; #, p<0.05; ###, p<0.001 *vs*. MI controls.

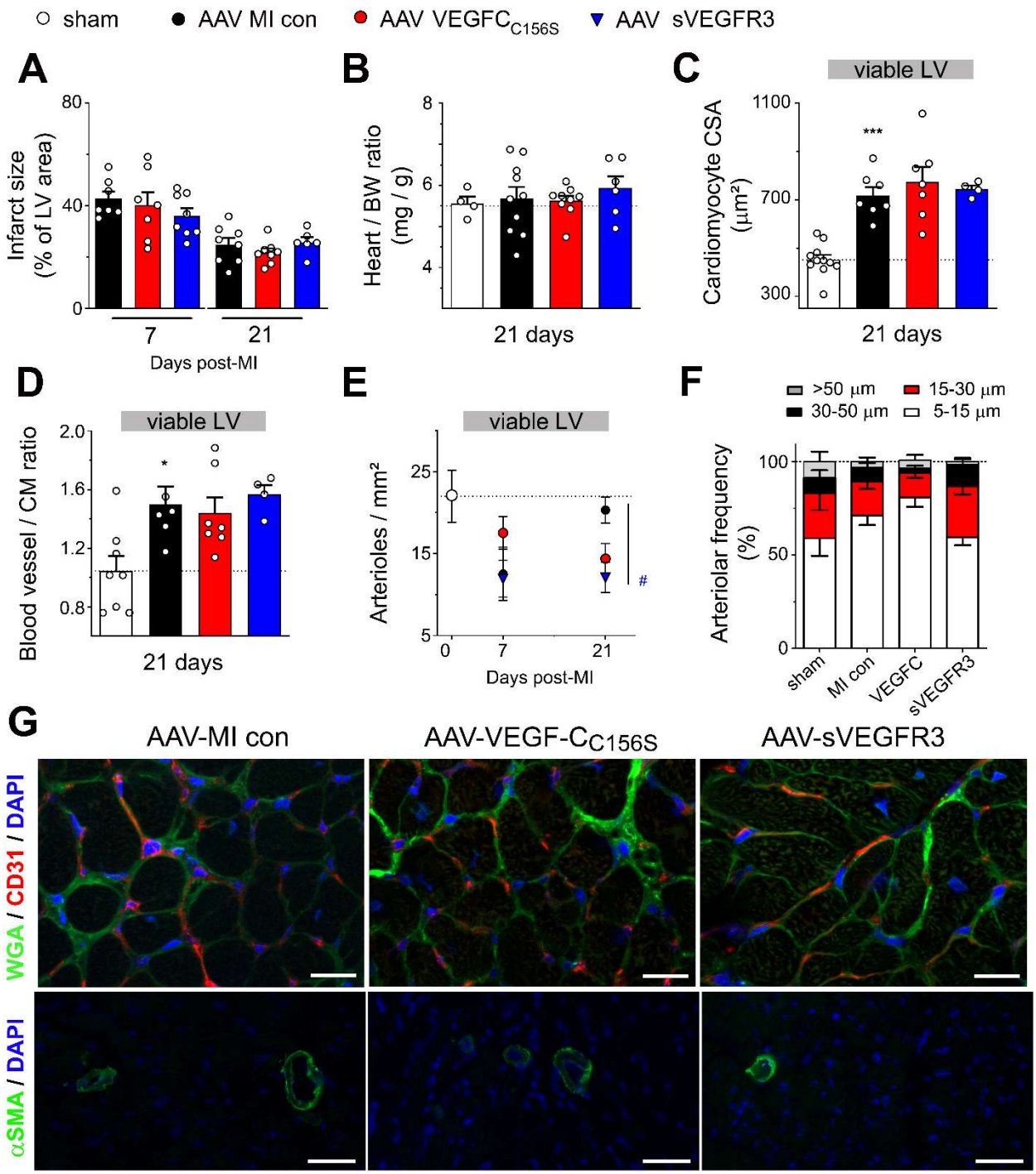

Suppl Fig. VI AAV delivery of VEGF-C$_{C156S}$ does not alter infarct sizes, cardiac hypertrophy, angiogenesis or arteriolar remodeling in mice post-MI, while sVEGFR3 reduces arteriogenesis

Infarct scar sizes (scar area % of LV) were determined by Sirius red staining of sequential cardiac sections (**a**). Cardiac hypertrophy at 21 days post-MI, evaluated as heart-to-body weight ratios (**b**), and as cardiomyocyte cross-sectional area (*CSA*, **c**) in the viable LV wall determined in wheat germ agglutinin-stained cardiac sections from healthy sham mice (*white, n=4-10*), MI controls (AAV-scramble, *black, n=6-10*), VEGFC (AAV-VEGF-C$_{C156S}$, *red, n=7-9*)

and sVEGFR3 (AAV-sVEGFR3, *blue, n=4-6*) treated mice. Cardiac angiogenesis in viable LV evaluated as $CD31^+$ blood vessel-to-cardiomyocyte ratios (**d**), and arterioles as αSMA^+ vessel density (**e**) complemented by arteriolar size-distribution profiling of arteriolar diameters at 21 days (**f**). Examples of blood vessel ($CD31^+$, *red*; upper row, *x40*) and arteriolar (αSMA^+, *green; bottom row, x20*) densities at 21 days post-MI (**g**). Scale bar = 20 µm upper row, 50 µm bottom row. Kruskal-Wallis nonparametric analysis, Dunn's posthoc test. *, $p<0.05$; ***, $p<0.001$ *vs*. sham; #, $p<0.05$ *vs*. MI control.

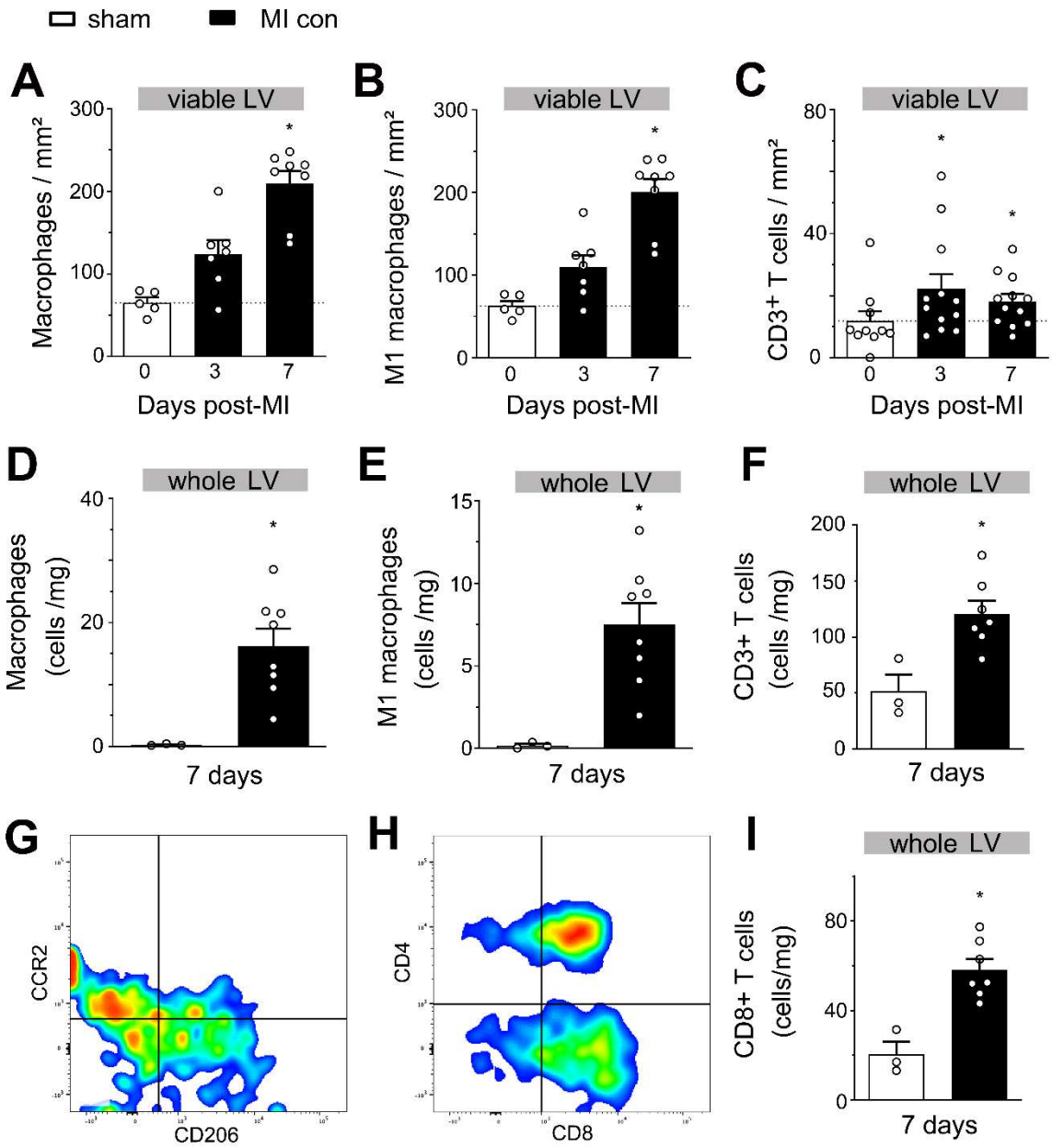

Suppl. Fig. VII Immunohistochemical and flow cytometric evaluations of cardiac immune cells in mice post-MI

Cardiac immune cell population dynamics were analyzed by immunohistochemistry at 3 and 7 days after MI to determine densities of $CD68^+$ macrophages (**a**), $CD206^-$ M1 type macrophage subpopulation (**b**), and $CD3^+$ T cells (**c**) in viable LV of MI mice (*black, n=7-8*) as compared to healthy sham mice (*white, n=5-6*). Cardiac immune cell levels in the whole LV were assessed by flow cytometry at 7 days post-MI (**d-i**) in healthy sham (*white, n=3*) and MI mice (*black, n=7-8*). Total macrophages were defined as $CD45^+$/ $CD11b^+$/ $MHCII^{low}$/ $F4\text{-}80^+$ cells (**d**) and M1 classical macrophages as $CCR2^+/CD206^-$ subpopulation (**e, g**). T lymphocytes were defined as $CD45^+$/ $CD3^+$/ $B220^-$ cells (**f**) and $CD8^+$ subpopulation as $CD4^-$/ $CD8^+$ subpopulation (**h, i**). Data reported as *cells/mg heart*. Mann Whitney U test: *, $p<0.05$ *vs*. sham.

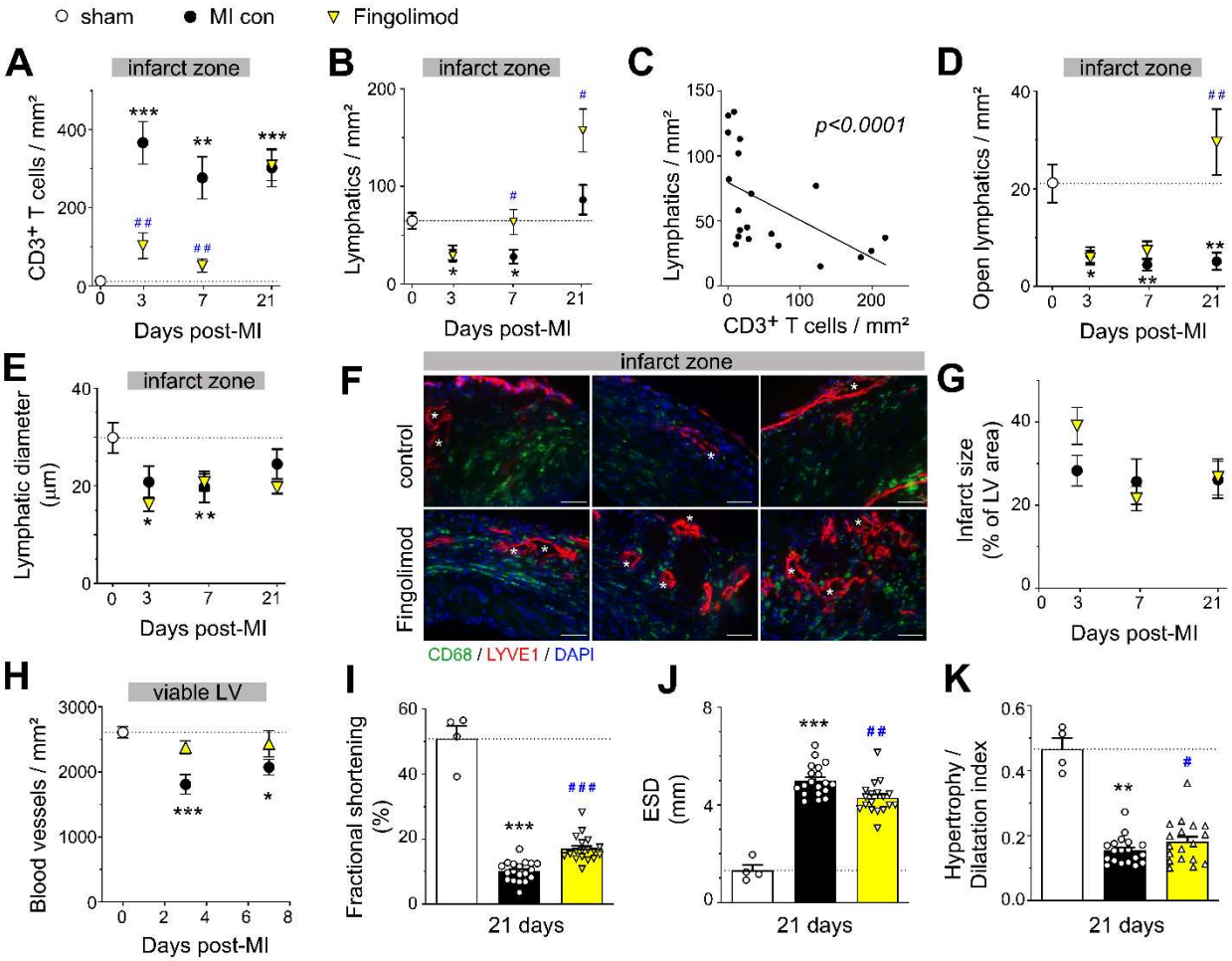

Suppl. Fig. VIII Suppression of cardiac T cell infiltration increases infarct lymphangiogenesis in mice post-MI

Infarct zone densities of $CD3^+$ total T cells (**a**) and lymphatic vessels (**b**) were analyzed by immunohistochemistry in MI controls (*black circles,* n=4-13 mice) and Fingolimod-treated MI mice (*yellow triangles,* n=7-9) at 3, 7 and 21 days post-MI. Healthy sham mouse levels are indicated by dashed line. Inverse linear correlation between cardiac lymphatic and T cell densities at 7 days post-MI. Spearman r=-0.71 (**c**). Analysis of infarct zone open lymphatic density (**d**) and lymphatic diameters (**e**). Examples of open lymphatics at 21 days (**f**). *x20*, scalebar = 50 µm. Asterix indicate open vessels. Quantification of infarct sizes (**g**) and blood vessel densities (**h**). Cardiac function analyzed by echocardiography at 21 days post-MI to determine LV fractional shortening (**i**), end-systolic LV diameter (*ESD*, **j**), and calculation of LV hypertrophy / dilatation index (**k**). Kruskal-Wallis followed by Dunn's posthoc test. *, p<0.05; **, p<0.01; ***, p<0.001 *vs*. sham; #, p<0.05; ##, p<0.01 *vs*. MI controls.

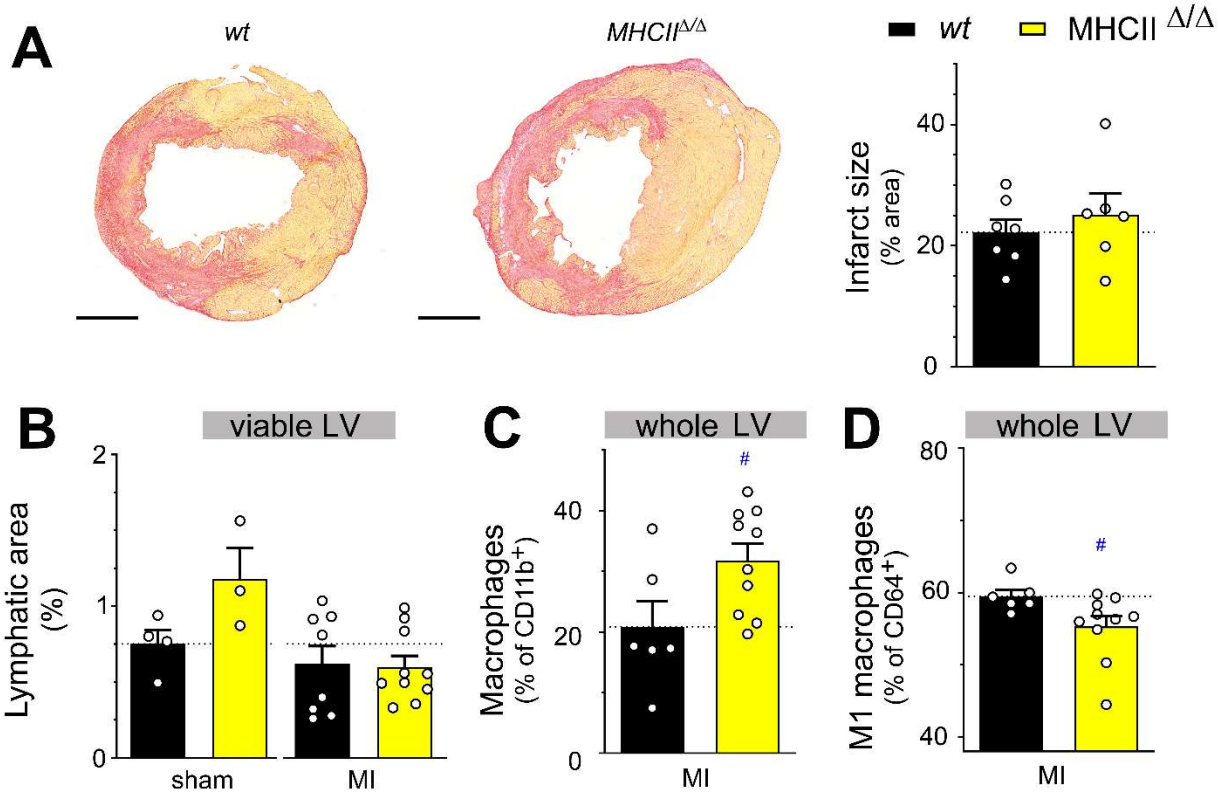

Suppl. Fig. IX Cardiac lymphatics and inflammation in CD4⁺ T cell-deficient mice post-MI

Examples and quantification of infarct scar size, visualized in Sirius Red stained sections, at 7 days post-MI in wildtype (*wt, black,* n=7-8) and MHCII$^{\Delta/\Delta}$ CD4⁺ T cell-deficient (*yellow*, n=6-10) mice (**a**). Scale bar = 1 mm. Quantification at 7 days post-MI of lymphatic vessel area (**b**) in viable LV wall in healthy (*sham*) versus post-MI hearts. Analysis by flow cytometry of total cardiac macrophages (CD64⁺ % of CD11b⁺) (**c**) and M1-type classical (CD86⁺/ CD206⁻) macrophage subpopulation (**d**) at 7 days post-MI. Comparison by Mann Whitney U test: #, p<0.05 *vs*. MI *wt* control.

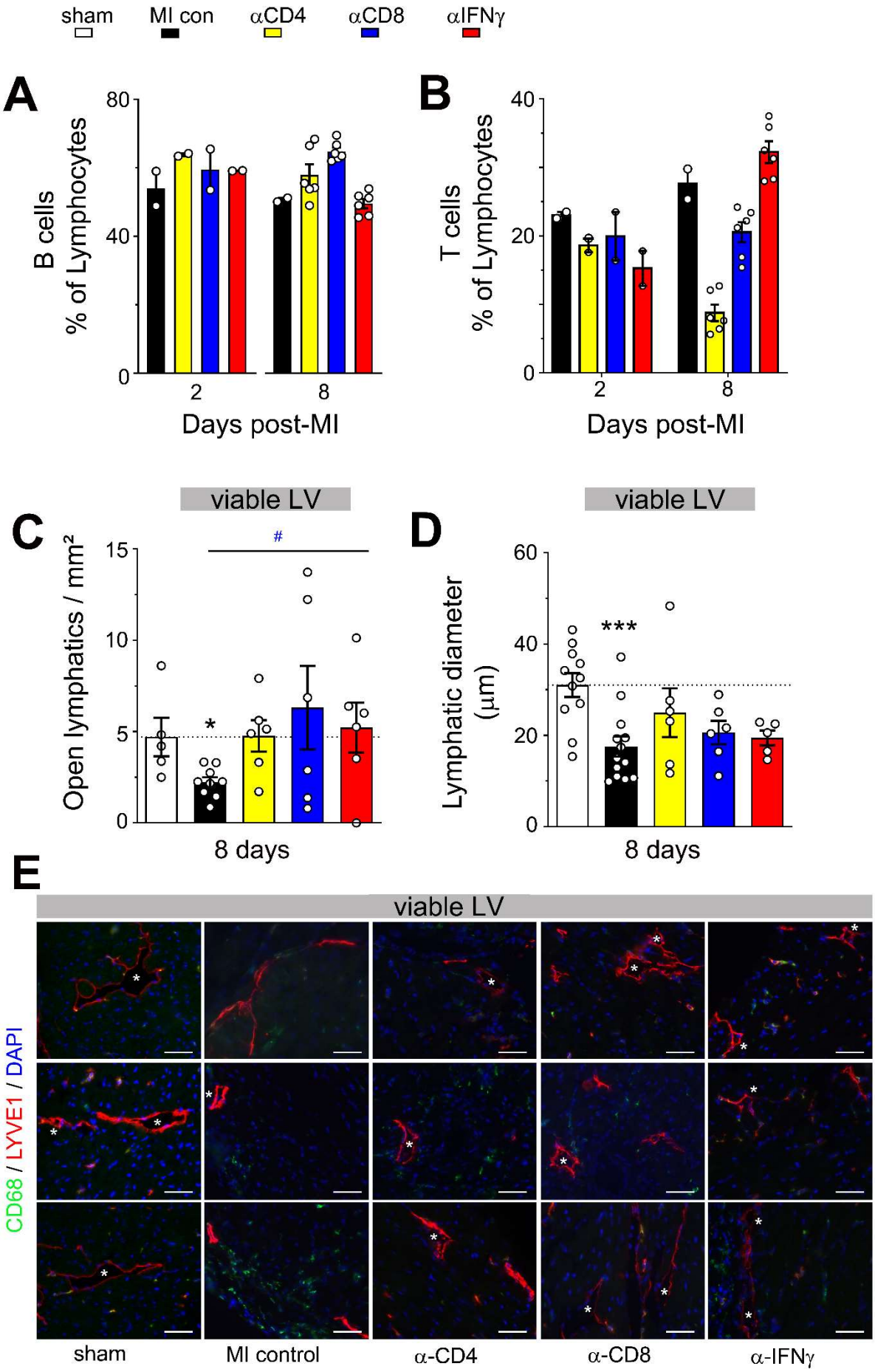
sham
MI con
αCD4
αCD8
αIFNγ
A
B cells
% of Lymphocytes
80
40
0
2
8
Days post-MI
B
T cells
% of Lymphocytes
40
20
0
2
8
Days post-MI
C
viable LV
Open lymphatics / mm²
15
10
5
0
#
*
8 days
D
viable LV
Lymphatic diameter (μm)
60
40
20
0
***
8 days
E
viable LV
CD68 / LYVE1 / DAPI
sham
MI control
α-CD4
α-CD8
α-IFNγ

Suppl. Fig. X Neutralization of IFNγ partially prevents rarefaction of open cardiac lymphatic vessels acutely post-MI without reducing B or T cell levels

Assessment by flow cytometry at 2 and 8 days post-MI of circulating $B220^+$ B cells (**a**) and $CD3^+$ T cells (**b**) in control MI mice (*black*, n=2), CD4-depleted mice (*yellow*, n=2-6), CD8-depleted mice (*blue*, n=2-6), and mice treated with an IFNγ-neutralizing antibody (*red*, n=2-6). Evaluation by immunohistochemistry of viable LV at 8 days post-MI of open lymphatic vessel density (**c**) and lymphatic diameters (**d**) in healthy sham (*white*, n= 5-11), control MI mice (*black*, n=10), CD4-depleted mice (*yellow*, n=6), CD8-depleted mice (*blue*, n=6), and anti-IFNγ-treated mice (*red*, n=7). Examples of open lymphatic vessel (*LYVE1*, red) slimming and rarefaction at 8 days post-MI (**e**). *x20*, scalebar = 50 µm. Asterix indicate open vessels. Kruskal-Wallis followed by Dunn's posthoc test. *, $p<0.05$ *vs*. sham; #, $p<0.05$ *vs*. MI controls.

Suppl Table I - Functional evaluation by echocardiography at 21 days post-MI

	MI saline con	**Fingolimod**	
	mean ± s.e.m	**mean** ± s.e.m	*vs. MI con*
AWT ED (mm)	0.55 ± 0.03	0.68 ± 0.04	*p<0.05*
AWT ES (mm)	**0.65 ± 0.02**	**0.86 ± 0.06**	*p<0.001*
AW FT (%)	21 ± 3	27 ± 4	*n.s*
LVEDD (mm)	5.6 ± 0.1	5.2 ± 0.2	*p=0.07*
LVESD (mm)	**5.0 ± 0.1**	**4.3 ± 0.2**	*p<0.01*
FS (%)	**10 ± 1**	**17 ± 1**	*p<0.001*
VTI (cm)	2.0 ± 0.1	2.0 ± 0.1	*n.s*
HR (bpm)	443 ± 10	443 ± 12	*n.s*
SV (mL/beat)	0.057 ± 0.002	0.057 ± 0.003	*n.s*
CO (mL/min)	25 ± 1	25 ± 2	*n.s*
CI (mL/min/g)	1.2 ± 0.0	1.2 ± 0.1	*n.s*

AWT ED, end-diastolic anterior wall thickness; AWT ES, end-systolic anterior wall thickness; AW FT, anterior wall fractional thickening; LVEDD, LV end-diastolic diameter; LVESD, LV end-systolic diameter; FS, LV fractional shortening; VTI, velocity-time integral; HR, heart rate; SV, stroke volume; CO, cardiac output; CI, cardiac index. N.S – non-significant. Two-tailed student's t-test.

Supplemental methods

Gene therapy vectors

Ad5 VEGF-C_{C1566S} and AAV9-sVEGFR3 vectors were produced as described [1,2]. To produce recombinant AAV9 vectors expressing human VEGF-C_{C1566S} the same construct as previously used to produce Ad5 VEGF-C_{C1566S} virus was used. Briefly, the expression cassette was subcloned into an AAV-vector and produced as described [3,2]. The AAV-vectors used are serotype 9, which efficiently transduces cardiomyocytes [4].

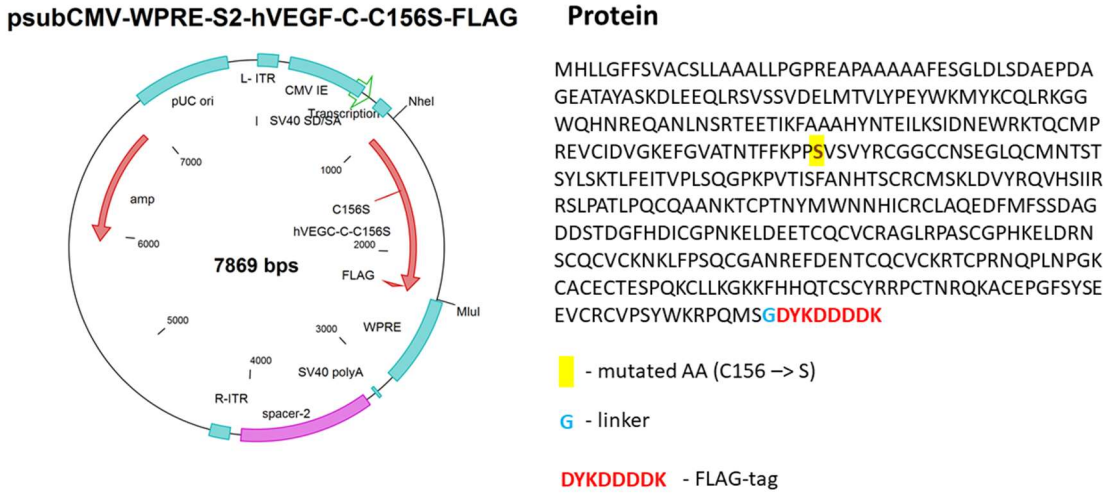

Experimental Models

Mouse MI model:

Left ventricular (LV) MI was induced in mechanically-ventilated anesthetized (Ketamine:100 mg/kg, Imalgene®, Merial; Xylazine:30 mg/kg, Rompun® 2%, Bayer Health Care) C57Bl/6J female mice or 20-22g C57Bl/6J female mice deficient for MHCII ($MHCII^{\Delta/\Delta}$ as a result of disruption of the IAβ gene) by permanent ligation of the left descending coronary artery as described [5]. We only used female mice for MI studies with the aim to compare our data to a previously published article on VEGF-C_{C156S} protein therapy where female mice were used[6]. In addition, female mice display lower mortality than male in the MI model which help us reduce the numbers of animals included in our studies. Buprenorphine (50 µg/kg, Buprecare®, Axcience) was injected subcutaneously 6 hours after surgery and twice per day until 3 days post-operation. Non-invasive echocardiography was performed as described [5] in sedated (Isoflurane 1.5%) mice using a Vivid 7 ultrasound echograph equipped with a M12L linear probe operating at 14MHz and outfitted with Echopac PC software (GE medical).

Rat MI model:

Myocardial infarction was induced in 200-220 g male Wistar rats by ligation of the left coronary artery (LCA), as described [4]. We used only male rats, as females may display more rapid LV

dilation as compared with males[7]. Echocardiography was performed before the operation, as well as 1 and 4 weeks after the operation by an operator blinded to the treatment groups. Transthoracic echocardiography in short axis M-mode was performed under isoflurane anesthesia with an Acuson Sequoia 512 Ultrasound System and an Acuson Linear 15L8 14 MHz transducer (Siemens Medical Solutions, Mountain View, CA, USA).

Prevention of T cell recruitment

Fingolimod (1mg/kg, FTY-720, Sigma-Aldrich) i.p pharmacological treatment was initiated immediately after MI with repeated injections on day 1 and 2 post-MI to prevent cardiac T cell recruitment acutely post-MI. MI controls received physiological saline i.p injections. Cardiac functional and cellular analyses at 3, 7 and 21 days post-MI were performed as described above. For depletion of specific T cell populations or cytokines, *InVivo*Mab antibodies (200 µg/mouse) were administered by repeated i.p injections on day 0 and 3 post-MI according to the manufacturer's instructions (BIO X CELL, New Hampshire, USA) using rat IgG2b,κ anti-mouse CD4 (clone G.K 1.5), rat IgG2b,κ anti-mouse CD8 (clone YTS 169.4), rat IgG1,κ anti-mouse IFNγ (XMG1.2), and mouse IgG2a,κ anti-mouse NK1.1 (clone PK136).

Immunohistochemistry

Mouse hearts

Cardiac sections were cut on a cryostat (8 µm or 30 µm thickness) and collected on SuperFrost plus glass slides. After fixation in acetone for 10 min, non-specific binding sites were blocked using Dako Diluent, followed by Biotin-Avidin Blocking kit (Thermo Scientific) when streptavidin (SA)-conjugates were used to detect biotinylated secondary antibodies. Primary antibodies (*see suppl table II*), diluted in blocking buffer, were incubated on the sections at r.t. for 1h, followed by repeated washing in PBS and incubation with secondary antibodies (*see suppl table III*) for 30 minutes to 1h. Double or triple stainings were performed sequentially, and negative controls included omission of primary antibodies. Slides were mounted in Vectashield containing DAPI, and images were acquired using x20 or x40 objectives on a Zeiss epifluorescence microscope (AxioImager J1) equipped with an apotome and Zen 2012 software (Zeiss). Images were analyzed by an operator blinded to the treatment groups using ImageJ software (NIH).

Suppl Table II – primary antibodies used for immunohistochemistry in mouse

antigen	article	supplier	species reactivity	host	dilution	Conc (µg/mL)
alpha SMA	*F3777*	Sigma Aldrich	mouse	mouse	1/100	**28**
CD3	*A0452*	DAKO	human, mouse	Rabbit	1/100	**6**
CD4	*13-0042-82*	eBioscience	mouse	rat	1/200	**2.5**
CD8a	*553028*	BD	mouse	rat	1/500	**1**
CD11c	14-0114-82	eBioscience	mouse	hamster	1/100	**5**
CD31/PECAM	*553371*	BD	mouse	rat	1/100	**0.6**
CD68	*14-0681-82*	eBioscience	mouse	rat	1/800	**5**
CD103	*13-1031-81*	eBioscience	mouse	hamster	1/100	**2**
F4/80	*MCA497R*	Abd Serotec	mouse	rat	1/200	**5**
FOXP3	*13-5773-80*	eBioscience	mouse	rat	1/250	**0.5**
ICAM	*14-0541-82*	eBioscience	mouse	rat	1/100	**2**
LYVE-1	*103-PA50*	Reliatech	mouse, rat	rabbit	1/1000	**0.4**
LYVE-1	*L5005*	Fitzgerald	mouse	rabbit	1/250	**0.05**
CD206/MRC1	*ab64693*	Abcam	mouse	rabbit	1/2500	**4**
Podoplanin	*14-5381-82*	eBioscience	mouse	hamster	1/10 000	**1**
Prox-1	*AF2727*	RnD system	human, mouse	goat	1/50	**4**
VEGFR3	*AF743*	RnD system	human, mouse	goat	1/200	**1**
VE-Cadherin	*AF1002*	RnD system	mouse	goat	1/200	**1**

Suppl Table III – secondary antibodies & reagents used for immunohistochemistry in mouse

antigen	article	supplier	Conc (µg/ mL)
Donkey anti-Rat Alexa Fluor 488	*712-545-153*	Jackson Immunoresearch	**3**
Donkey anti-Rat Cy3	*712-166-153*	Jackson Immunoresearch	**3**
Goat anti-Rat Alexa Fluor 647	*A-21247*	Thermo Fisher Scientific/ Invitrogen	**0.8**
Donkey anti-Rabbit Cy3	*711-165-152*	Jackson Immunoresearch	**3**
Donkey anti-Rabbit Alexa Fluor 647	*711-605-152*	Jackson Immunoresearch	**1.5**
Donkey anti-Goat DYLIGHT 550	*A50-201D3*	Interchim	**1.3**
Donkey anti-Goat DYLIGHT 488	*A50-201D2*	Interchim	**1.3**
Streptavidin-FluoProbes 647	*FP-CA5640*	Interchim fluoprobes	**0.7**
Streptavidin-FluoProbes 547H	*FP-CA5570*	Interchim fluoprobes	**0.7**
Goat anti-Hamster Alexa Fluor 488	*A-21110*	Thermo Fisher Scientific / Invitrogen	**0.8**

Rat hearts

Frozen rat cardiac sections were stained with mouse anti-rat RECA-1 (MCA970, Serotec), goat-anti-mouse VEGFR3 (*#AF743*, R&D Systems), goat antihuman Prox1 (*#AF2727*, R&D Systems), and Lyve1 (rabbit-anti-mouse, *produced in-house*) antibodies. Alexa Fluor 488- and 594- conjugated secondary antibodies (Molecular Probes, Thermo Fisher) were used for detection. Slides were imaged with AxioImager fluorescent microscope (Zeiss) and area percentage of the vessels were quantified using ImageJ software (NIH).

Image analysis of cardiac sections

Lymphatic vessels were defined as strongly Lyve1-positive structures, lacking macrophage markers (F4/80 or CD68), but positive for podoplanin, Prox1, and VEGFR3. Lymphatics are preferentially located in the subepicardium in rodent hearts. These Lyve1-positive, F4/80 or CD68-negative vessels clearly differed from $CD68^+$ or $F4\text{-}80^+$ macrophages that either lacked or displayed weaker Lyve1 signal. However, some large, rounded $CD68^+$ macrophages were strongly positive for Lyve1, notably in the infarct (see **Fig 2d**). These macrophages, also differing in size and morphology from the elongated cell body and nucleus typical of lymphatic endothelial cells, were readily excluded from lymphatic counts. Photos were captured at *x20* or *x40*.

Searching for a distinguishing molecular marker, we analyzed the spatial distribution of podoplanin versus lyve1 expression in cardiac lymphatics. We found that in healthy mice there may be a preference for podoplanin expression in precollectors, rather than in capillary segments. However, this distribution is not sufficiently consistent to allow unambiguous 2D discrimination of precollectors in tissue sections. Due to this absence of conclusive markers to distinguish precollectors from capillaries, we have made use of the fact that precollectors preferentially run in a base-to-apex fashion, whereas lymphatic capillaries lack such consistent spatial organization. Hence, by evaluating vessels with a lumen parallel to horizontal cardiac sections, we argued that the precollector population of vessels will be more frequently detected as vessels running perpendicular to the section (= open lumen vessels).

To assess the size and frequency of open lymphatic vessels (diameter > 5 µm; a population enriched in precollector vessels), between 10-20 images from the LV freewall, and from the infarct zone were collected and analyzed for each mouse. The density (**open vessels/mm²**) and lymphatic vessel lumen sizes were measured and used to calculate **mean vessel diameter**. The parameter **% open lymphatic area** was calculated as the sum total of all measured lymphatic diameters divided by the total cardiac area analyzed for each mouse heart. On average for each mouse, 0.93 ±0.1 mm² of the LV was analyzed to determine lymphatic vessel sizes and % open lymphatic area.

Percentage of proliferating lymphatic vessels was calculated as the number of lymphatic vessels containing at least one proliferating Ki67^{+} lymphatic endothelial cell nuclei divided by the total number of lymphatics in each image. Only nuclei in lymphatic vessels double positive for DAPI and Ki67 were counted to determine lymphatic endothelial cell proliferation.

Blood vessels were defined as strongly CD31-positive structures. These clearly differed from lymphatic vessels that either lacked or displayed weaker CD31 signal. Blood to cardiomyocyte ratios were evaluated in sections double stained for CD31 and WGA imaged at *x40*. Individual endothelial cells were not counted, rather vessels structures were assessed. If two vessels were adjacent and partly overlapping, they were counted as two vessels. For one vessel that divides into two branches, two vessels were counted.

Arterioles were defined as smooth muscle actin-positive vessels. Images were captured at *x20*. Cardiac macrophages were defined as CD68 or F4/80 positive cells. M2-like macrophages were defined as CD206 (MMR) positive, and M1 type macrophages as CD206 negative macrophages. Total T cells were defined as CD3 positive cells, divided into CD8a positive or CD4 positive cells. Images were captured at *x20*.

Histology

Cardiac cryosections (8 µm) of mouse hearts were processed for Sirius Red staining as described [5]. Infarct sizes were evaluated in 4-5 sections spanning the LV, and calculated as: (%) Infarct area/ total LV area. Cardiac interstitial collagen density ("*fibrosis"*) was evaluated in Sirius Red-stained sections imaged on a light microscope (Zeiss) equipped with an *x20* objective. Image analysis was performed using ImageJ software (NIH).

VEGF-C plasma levels

Plasma VEGF-C levels were measured using a human VEGF-C ELISA Kit (R&D Biosystems, DVEC00) according to manufacturer's instructions.

Real-Time Polymerase Chain Reaction

Cardiac samples were collected at 3 weeks after MI. RNA extraction was performed with Trizol method. RNA quality was analyzed by Nanodrop 2000 (Thermo Fisher Scientific). Real-time polymerase chain reaction was performed on a LightCycler (Roche Molecular Biochemicals) with a commercially available mix (FastStart DNA Master SYBR Green I kit; Roche). The primer sequences are listed in suppl *table IV.* Gene expression levels were calculated for each animal as numbers of cycles for the gene of interest normalized to B2m house-keeping gene. Healthy sham animal ratios are then set as 100%, and values in MI con or VEGF-C-treated mice are expressed relative to healthy sham.

Suppl Table IV – RT-PCR primers used for cardiac expression analyses in mouse

gene	sense	antisense	amplicon (bp)
B2m	GCTGCTACTCGGCGCTTCA	GCAGGCGTATGTATCAGTCTCAGT	343
mCcl2	CCCAATGAGTAGGCTGGAGA	GCTGAAGACCTTAGGGCAGA	210
mCcl21	TCCCTACAGTATTGTCCGAGGC	ATCAGGTTCTGCACCCAGCCTT	141
mCx3cl1	CAGTGGCTTTGCTCATCCGCTA	AGCCTGGTGATCCAGATGCTTC	149
mFlt4 (Vegfr3)	AGACTGGAAGGAGGTGACCACT	CTGACACATTGGCATCCTGGATC	128
mLyve1	ACCAGGTAGAGTCAGCGCAGAA	CAGGACACCTTTGCCATTCTTCC	128
mPdpn	ACAACCACAGGTGCTACTGGAG	GTTGCTGAGGTGGACAGTTCCT	116
mVegfc	AGCCCACCCTCAATACCAG	GCTGCTCCAAACTCCTTCC	154
hVEGFC	TACAGACGGCCATGTACGAA	GCTCATTTGTGGTCTTTTCC	108
mVegfd	CTCCACCAGATTTGCGGCAACT	ACTGGCGACTTCTACGCATGTC	112

Whole mount

Prior to sacrifice, deeply anesthetized mice were perfused with warm saline solution, followed by perfusion-fixation with warm 3% paraformaldehyde (PFA). Hearts were removed and postfixed (3% PFA) for 7h. Following dehydration in graded methanol baths, and post-fixation in Dent's fixative, samples were bleached in graded H_2O_2 baths. After extensive blocking of non-specific binding sites and tissue permeation with Triton-X100, cardiac lymphatics were revealed using Lyve1 (rabbit polyclonal, Reliatech, *1/500*), followed by a fluorescence-coupled secondary antibody (Cy5-conjugated donkey anti-rabbit, *1/500)*. Arterioles were revealed using anti-αSMA antibodies (Cy3-conjugated mouse monoclonal antibody, Sigma-Aldrich, *#C6198*, *1/200*). Extensive washing was performed to remove nonspecific binding. Hearts were clarified using a modified iDISCO+ protocol, as described [8], based on incubation in graded methanol baths followed by incubation in dichloromethane (DCM, Sigma-Aldrich, *#270997-12X100ML*) and dibenzyl ether (DBE, Sigma-Aldrich, *#108014-1KG*) before light sheet and confocal imaging.

3D Imaging and Image Processing

3D imaging was performed by light sheet microscopy as described [8]. Acquisitions were performed with an ultramicroscope II (LaVision BioTec) using the ImspectorPro software (LaVision BioTec). The light sheet was generated by a laser (wavelengths 561 or 640 nm, Coherent Sapphire Laser, LaVision BioTec) focused using two cylindrical lenses. Two adjustable protective lenses were applied for small or large working distances. A binocular stereomicroscope (MXV10, Olympus) with an *x*2 objective (MVPLAPO, Olympus) was used at different magnifications (*x*0.8 and *x*4). The corresponding zoom factors and numerical apertures are available at:
http://www.lavisionbiotec.com/products/UltraMicroscope/specification.html

Samples were placed in an imaging reservoir made of 100% quartz (LaVision BioTec) filled with DBE and illuminated from the side by the laser light sheet. A PCO Edge SCMOS CCD camera (2560× 2160 pixel size, LaVision BioTec) was used to capture images. The step size between each image was fixed at 1 or 2 µm. All tiff images were generated in 16-bit.

For confocal laser scanning microscopy, imaging was performed with an upright fixed-stage TCS SP8 confocal microscope (Leica Microsystems, France) equipped with multiple laser lines (wavelengths 561 or 640 nm). In order to acquire deep confocal views, a *x25* objective was used (numerical aperture 0.95, working distance 2500 µm, water immersion). Images were captured using a hydrid detector (Hamamatsu) in photon counting z-stack mode.

Image Processing

Images, 3D volume, and movies were generated using Imaris x64 software (version 8.0.1, Bitplane). Z stack light sheet images were first converted to imaris file (.ims) using ImarisFileConverter and 3D reconstruction was performed using the "volume rendering" function. To facilitate image processing, images were converted to 8-bit format. Optical slices were obtained using the "orthoslicer" tool. 3D pictures and movies were generated using the "snapshot" and "animation" tools. Movie reconstruction with .tiff series were performed with NIH ImageJ (1.50e, Java 1.8.0_60, 64-bit).

Z stack confocal raw data images were deconvoluted through image processing with Huygens professional software (SVI, The Netherlands). Maximal intensity projection views were generated with Fiji Image J[9] software (1.51u, Java 1.8.0_66, 64-bit).

Flow Cytometry

Blood samples:

Blood was harvested from abdominal aorta into EDTA blood collection tubes. Red blood cells were lysed using RBC lysis buffer (eBiosciences, *#00-4333-57*) incubation for 10 minutes at r.t. The reaction was stopped by adding 10 mL cold FACS buffer (PBS 1X without Ca^{2+} or Mg^{2+}, 1% BSA and 3 mM EDTA). 100 µL blood per mouse was incubated with 1 µL Fc-Block (BD Pharmingen, *#553142*) for 15 minutes at 4°C. Cells were then incubated for 20 minutes at r.t in specific antibody cocktails designed to analyze lymphocyte and myeloid cell populations (see suppl *table V*). Tubes were centrifuged to eliminate supernatants and cells were resuspended in 600 µL FACS buffer.

Cardiac samples:

Prior to sacrifice, deeply anesthetized mice were perfused with warm saline solution, the heart was removed and the left ventricle, including both scar and viable LV were cut into small pieces. Single cell suspensions were prepared by incubation in tissue-dissociating solution

(125 U/mL collagenase type XI, *#C7657*, Sigma; 450 U/mL collagenase type I, *#C0130*, Sigma; 60 U/mL hyaluronidase type I, *#H3506*, Sigma; and 60 U/mL DNase 1 *#DN25*, Sigma) [10,11] coupled to gentleMACS Dissociator (MACS; Miltenyi Biotec, Auburn, CA). Digested tissues were washed with DMEM culture medium and filtered to remove undigested tissue pieces (80 µm mesh, and 40 µm mesh, BD Biosciences). Single cell suspensions were made in 100 µL FACS buffer.

To block nonspecific binding of antibodies to Fcγ receptors, isolated cells were first incubated with Fc-Block for 15 minutes at 4°C. Subsequently, cells were stained with specific antibody cocktails (see suppl *table V*) for 20 minutes at r.t, followed by washing with FACS buffer and resuspension in 600 µL FACS buffer. To quantify immune cells per mL blood or per mg heart, 103 300 fluobeads (Flow-count Fluorospheres, Beckman coulter *#7547053*) was added to each samples prior to analysis. Flow cytometry was performed on a 12-color **LSRFortessa** (BD Biosciences) followed by analysis using FlowJo software (TreeStar, Inc, San Carlos, CA). Results are expressed as % of parent population or as immune cells per mL blood or per mg heart tissue, respectively.

Suppl Table V – primary antibodies used for flow cytometry analyses in mouse

Antigen	Source & catalogue #
Rat anti-mouse CD16/32 (Fc block)	BD Pharmingen 553142
eFluor™ 455UV Fixable Viability Dye	ebioscience 65-0868-14
PerCP anti-mouse CD45	Sony Biotechnology 1115650
APC/Cy7 anti-mouse Ly-6C	Sony Biotechnology 1240130
FITC anti-mouse CD11b	BD Pharmingen 553310
PE anti-mouse CD115 (CSF-1R)	Sony Biotechnology 1277530
Brillant Violet 605 anti-mouse F4/80	Sony Biotechnology 1215665
Brillant Violet 650 anti-mouse CD86	Sony Biotechnology 1125175
Alexa Fluor 700 anti-mouse MHCII (I-A/I-E)	Sony Biotechnology 1138110
APC anti-mouse CD206 (MMR)	Sony Biotechnology 1308540
PE/Cy7 anti-mouse CD192 (CCR2)	Sony Biotechnology 1353060
Brillant Violet 421 anti-mouse CX3CR1	Sony Biotechnology 1345115
PE anti-mouse CD45R (B220)	BD Pharmingen 553090
APC anti-mouse CD3	BD Pharmingen 553142
APC/Cy7 anti-mouse CD4	Sony Biotechnology 1102070
Alexa Fluor 700 anti-mouse CD8a	Sony Biotechnology 1103650
Alexa Fluor 488 anti-mouse FoxP3	Sony Biotechnology 2200055
Brillant Violet 605 anti-mouse CD206	Biolegend clone MCA2235F
APC anti-mouse CD86	Biolegend clone GL1
PE-Cy7 anti-mouse CD64	Biolegend clone X54-5/7.1
Percp Cy5.5 anti-mouse LY6G	Biolegend clone 1A8
Pacific blue anti-mouse CD11b	Biolegend clone M1/70

References

1. Antila S, Karaman S, Nurmi H, Airavaara M, Voutilainen MH, Mathivet T, Chilov D, Li Z, Koppinen T, Park J-H, Fang S, Aspelund A, Saarma M, Eichmann A, Thomas J-L, Alitalo K. Development and plasticity of meningeal lymphatic vessels. *J Exp Med*. 2017;214(12):3645-3667. doi:10.1084/jem.20170391.

2. Visuri MT, Honkonen KM, Hartiala P, Tervala TV, Halonen PJ, Junkkari H, Knuutinen N, Ylä-Herttuala S, Alitalo KK, Saarikko AM. VEGF-C and VEGF-C156S in the pro-lymphangiogenic growth factor therapy of lymphedema: a large animal study. *Angiogenesis*. 2015;18(3):313-326. doi:10.1007/s10456-015-9469-2.

3. Anisimov A, Alitalo A, Korpisalo P, Soronen J, Kaijalainen S, Leppänen V-M, Jeltsch M, Ylä-Herttuala S, Alitalo K. Activated forms of VEGF-C and VEGF-D provide improved vascular function in skeletal muscle. *Circ Res*. 2009;104(11):1302-1312. doi:10.1161/CIRCRESAHA.109.197830.

4. Kivelä R, Bry M, Robciuc MR, Räsänen M, Taavitsainen M, Silvola JMU, Saraste A, Hulmi JJ, Anisimov A, Mäyränpää MI, Lindeman JH, Eklund L, Hellberg S, Hlushchuk R, Zhuang ZW, Simons M, Djonov V, Knuuti J, Mervaala E, Alitalo K. VEGF-B-induced vascular growth leads to metabolic reprogramming and ischemia resistance in the heart. *EMBO Mol Med*. 2014;6(3):307-321. doi:10.1002/emmm.201303147.

5. Besnier M, Galaup A, Nicol L, Henry J-P, Coquerel D, Gueret A, Mulder P, Brakenhielm E, Thuillez C, Germain S, Richard V, Ouvrard-Pascaud A. Enhanced angiogenesis and increased cardiac perfusion after myocardial infarction in protein tyrosine phosphatase 1B-deficient mice. *FASEB J Off Publ Fed Am Soc Exp Biol*. 2014;28(8):3351-3361. doi:10.1096/fj.13-245753.

6. Klotz L, Norman S, Vieira JM, Masters M, Rohling M, Dubé KN, Bollini S, Matsuzaki F, Carr CA, Riley PR. Cardiac lymphatics are heterogeneous in origin and respond to injury. *Nature*. 2015;522(7554):62-67. doi:10.1038/nature14483.

7. Chen Y-F, Redetzke RA, Sivertson RM, Coburn TS, Cypher LR, Gerdes AM. Post-myocardial infarction left ventricular myocyte remodeling: are there gender differences in rats? *Cardiovasc Pathol Off J Soc Cardiovasc Pathol*. 2011;20(5):e189-195. doi:10.1016/j.carpath.2010.09.007.

8. Belle M, Godefroy D, Couly G, Malone SA, Collier F, Giacobini P, Ch?dotal A. Tridimensional Visualization and Analysis of Early Human Development. *Cell*. 2017;169(1):161-173.e12. doi:10.1016/j.cell.2017.03.008.

9. Schindelin J, Arganda-Carreras I, Frise E, Kaynig V, Longair M, Pietzsch T, Preibisch S, Rueden C, Saalfeld S, Schmid B, Tinevez J-Y, White DJ, Hartenstein V, Eliceiri K, Tomancak P, Cardona A. Fiji: an open-source platform for biological-image analysis. *Nat Methods*. 2012;9(7):676-682. doi:10.1038/nmeth.2019.

10. Nahrendorf M, Swirski FK, Aikawa E, Stangenberg L, Wurdinger T, Figueiredo J-L, Libby P, Weissleder R, Pittet MJ. The healing myocardium sequentially mobilizes two monocyte subsets with divergent and complementary functions. *J Exp Med*. 2007;204(12):3037-3047. doi:10.1084/jem.20070885.

11. Barbay V, Houssari M, Mekki M, Banquet S, Edwards-L?vy F, Henry J-P, Dumesnil A, Adriouch S, Thuillez C, Richard V, Brakenhielm E. Role of M2-like macrophage recruitment during angiogenic growth factor therapy. *Angiogenesis*. 2015;18(2):191-200. doi:10.1007/s10456-014-9456-z.

Major Resources Tables

Animals (in vivo studies)

Species	Vendor or Source	Background Strain	Sex
mouse	Janvier Laboratories, France	C57Bl/6J	Female
mouse	Inserm UMR1048, Université de Toulouse III, Toulouse	C57Bl/6J, *wt*	Female
mouse	Inserm UMR1048, Université de Toulouse III, Toulouse	C57Bl/6J, MHCII$^{\Delta/\Delta}$	Female
rat	Harlan/Envigo	Wistar rats (RccHan:WIST)	Male

Antibodies

Target antigen	Vendor	Catalog #	Working concentration (µg /mL)
alpha SMA	Sigma Aldrich	*F3777*	**28**
CD3	DAKO	*A0452*	**6**
CD4	eBioscience	*13-0042-82*	**2.5**
CD8a	BD	*553028*	**1**
CD11c	eBioscience	14-0114-82	**5**
CD31/PECAM	BD	*553371*	**0.6**
CD68	eBioscience	*14-0681-82*	**5**
CD103	eBioscience	*13-1031-81*	**2**
F4/80	Abd Serotec	*MCA497R*	**5**
FOXP3	eBioscience	*13-5773-80*	**0.5**
ICAM	eBioscience	*14-0541-82*	**2**
LYVE-1	Reliatech	*103-PA50*	**0.4**
LYVE-1	Fitzgerald	*LR005*	**0.05**
CD206/MRC1	Abcam	*ab64693*	**4**
Podoplanin	eBioscience	*14-5381-82*	**1**
Prox-1	RnD system	*AF2727*	**4**
VEGFR3	RnD system	*AF743*	**1**
VE-Cadherin	RnD system	*AF1002*	**1**

Target antigen	Vendor	Catalog #	Working concentration (µg /mL)
Donkey anti-Rat Alexa Fluor 488	Jackson Immunoresearch	*712-545-153*	**3**
Donkey anti-Rat Cy3	Jackson Immunoresearch	*712-166-153*	**3**
Goat anti-Rat Alexa Fluor 647	Thermo Fisher Scientific/ Invitrogen	*A-21247*	**0.8**
Donkey anti-Rabbit Cy3	Jackson Immunoresearch	*711-165-152*	**3**
Donkey anti-Rabbit Alexa Fluor 647	Jackson Immunoresearch	*711-605-152*	**1.5**
Donkey anti-Goat DYLIGHT 550	Interchim	*A50-201D3*	**1.3**
Donkey anti-Goat DYLIGHT 488	Interchim	*A50-201D2*	**1.3**

Streptavidin-**FluoProbes 647**	Interchim fluoprobes	*FP-CA5640*	**0.7**
Streptavidin-F**luoProbes 547H**	Interchim fluoprobes	*FP-CA5570*	**0.7**
Goat anti-Hamster Alexa Fluor 488	Thermo Fisher Scientific / Invitrogen	*A-21110*	**0.8**